JJ

Institut
de Physique
Nucléaire
de Lyon

Université Claude Bernard

IN2P3 - CNRS

LYCEN 9611
Avril 1996

Study of K-REC with bare 60 MeV/u Kr ions channeled in a Si crystal. Experiments and simulations.

S. Andriamonje[1], M. Chevallier[2], C. Cohen[3], N. Cue[4], D. Dauvergne[2], J. Dural[5], F. Fujimoto[6], R. Kirsch[2], A. L'Hoir[3], J.C. Poizat[2], Y. Quéré[6], J. Remillieux[2], C. Röhl[1], H. Rothard[5], J.P. Rozet[3], D. Schmaus[3], M. Toulemonde[5] and D. Vernhet[3]

[1]*Centre d'Etudes Nucléaires de Bordeaux-Gradignan/IN2P3, le Haut-Vigneau, 33175 Gradignan cedex, France*

[2]*Institut de Physique Nucléaire de Lyon, IN2P3/CNRS, Université Claude Bernard, F-69622 Villeurbanne cedex, France*

[3]*Groupe de Physique des Solides, CNRS/URA 017, Université Paris VII et Paris VI, 75251 Paris cedex 05, France*

[4]*Department of Physics, The Hong Kong University of Science and Technology, Kowloo, Hong Kong*

[5]*C.I.R.I.L., UMR 11 CNRS/CEA, rue Claude Bloch 14040 Caen cedex, France*

[6]*Laboratoire des Solides Irradiés, Ecole Polytechnique, 91128 Palaiseau cedex, France*

to be published in Phys. Rev. A

43, Boulevard du 11 Novembre 1918 - 69622 VILLEURBANNE Cedex - France

Study of K-REC with bare 60 MeV/u Kr ions channeled in a Si crystal. Experiments and simulations.

S. Andriamonje[1] M. Chevallier[2] C. Cohen[3] N. Cue[4]
D. Dauvergne[2] J. Dural[5] F. Fujimoto[6] R. Kirsch[2]
A. L'Hoir[3] J.-C. Poizat[2] Y. Quéré[6] J. Remillieux[2]
C. Röhl[1] H. Rothard[5] J.P. Rozet[3] D. Schmaus[3]
M. Toulemonde[5] and D. Vernhet[3].

April 30, 1996

[1] Centre d'Etudes Nucléaires de Bordeaux- Gradignan and IN2P3, le Haut-Vigneau, 33175 Gradignan Cedex, France

[2] Institut de Physique Nucléaire de Lyon and IN2P3, Université Claude Bernard Lyon-I, 43, Bd du 11 Novembre 1918, 69622 Villeurbanne Cedex, France

[3] Groupe de Physique des Solides, CNRS URA 017, Université Paris VII et Paris VI, 75251 Paris Cedex 05, France

[4] Department of Physics, The Hong Kong University of Science and Technology, Kowloon, Hong Kong

[5] C.I.R.I.L., UMR 11 CNRS-CEA, rue Claude Bloch, 14040 Caen Cedex, France

[6] Laboratoire des Solides Irradiés, Ecole polytechnique, 91128 Palaiseau Cedex, France

PACS numbers : 61.85.+p, 34.70.+e, 34.80.Lx

Abstract

We have performed K-shell Radiative Electron Capture (K-REC) measurements with bare 60.1 MeV/u incident krypton ions, both in channeling conditions and for random orientation of a 37 μm silicon crystal. The sampled electron densities are quite different in each case, which has an influence both on the shape and on the amplitude of the K-REC photon peak. We have developped simulations of the K-REC photon lines : for this we have determined the impact parameter distribution at statistical equilibrium for various beam incidence conditions (direction and angular spread) using the continuum potential model for channeled ions. Multiple scattering effects were included. The K-REC photon peak was calculated within the non-relativistic dipole approximation, K-REC being assumed to be a purely local process. Solid state electron densities were used, and impact parameter dependent electron momentum distributions (Compton profiles) were calculated for 2s and 2p silicon electrons.

A remarkable agreement is found between the spectra measured with very high statistics, and the calculated ones, which leads to the following results : i) the dependence of the K-REC yield on the beam incidence angle is obtained separately for silicon core and valence electrons, which was never observed before. We find that the core electron contribution to REC is still significant for axial alignment, whereas it is generally neglected in the litterature. ii) Electron Compton profiles are found to vary significantly with impact parameter. iii) The free electron gas model represents a fair approximation for the description of valence electron Compton profiles. iv) The K-REC cross section is measured with an absolute accuracy better than 20 %, and found to be close to the value calculated within the non-relativistic dipole approximation.

1 Introduction

Channeling of swift heavy ions in thin crystals can be used as a tool for suppressing the interaction between the projectile and the atomic cores of a solid target. Interaction with conduction and valence electrons of the crystal becomes observable, and even dominant. Thus channeling allows the observation of charge exchange processes between highly stripped heavy ions and quasi-free electrons, i.e. which involve no recoil of the target atom : this is the case for Radiative Electron Capture (REC) [1, 2, 3] in which electron capture is accompanied by the emission of a photon, Resonant Transfer and Excitation (RTE) [4, 5, 6, 7] in which the capture is accompanied by the resonant electronic excitation of the projectile, and Electron Impact Ionization (EII) [8, 9]. Moreover, through the study of such localized processes, channeling can be used to get more information about the local electronic structure in a crystal.

Basically an axially channeled ion can be seen like a particle trapped in a *2-D* potential, that is the transverse potential, averaged along the atomic rows. Then the transverse energy of the ion inside the crystal determines the accessible transverse space for the trajectory, and then the mean electron density sampled by the ion. As studied in details by L'Hoir et al. [9], one can connect the energy loss rate and the charge state at emergence of a channeled ion to its transverse energy. However, since energy loss is not a purely local process [10], the determination of the densities of target electrons in various states sampled by channeled ions remains a major problem in the interpretation of experiments devoted to a charge exchange process in channeling conditions. If the process studied is also observable in random conditions (for which all electrons of the crystal may participate with the same probability), the comparison of random and aligned experiments should allow one to extract the specific contributions of each type of target electrons.

The momentum distribution of electrons (Compton profile) reflects the dispersion of the

kinetic energy of the target electrons. For instance it is wider for K-shell electrons than for valence or conduction electrons. These distributions are connected to the electron wave functions and densities. Then the studies of charge exchange processes taking place at well defined distances from atomic strings should provide additional information on the local electron density through the corresponding electron Compton profile, and then allow a more detailed confrontation of experiment with the theoretical description of electron structure in solids. Both RTE and REC are processes which imply large momentum transfer for the captured electron. They are then expected to be "local" processes, and thus, in principle, able to give information on local electron densities and Compton profiles. Compton profiles can be deduced from RTE through the study of resonance shapes, and from REC through the study of the photon line shapes. However, in RTE experiments - KLL-RTE especially [6, 11, 7] - the fine structure of the resonance is a limiting factor for a precise study of the line shape and then of the Compton profile of the target electrons (except for the lightest and heaviest ions for which the resonance structure is either negligible or dominant with respect to the Compton profile). K-REC is a much more attracting case for the two following reasons : REC is a non-resonant process, which makes it easier to observe experimentally, and K-REC is monoenergetic. The K-REC shape has been already used for determining electron densities by Datz et al. [11] and by Miraglia et al. [12] in their interpretation of a previous experiment by Appleton et al. [1]. In these works the contribution of core electrons to the K-REC line shape could not be evaluated, in particular because K-REC could not be observed in random conditions.

The aim of this work is the study of K-shell radiative capture by bare channeled ions. The K-REC line shape has been studied as a function of the crystal orientation, i.e. of the transverse energy distribution of the incident ions along the crystal axis. A few years ago, we had already observed K and L-REC with hydrogen-like 25 MeV/u Xe^{53+} ions channeled in a Si crystal [2]. However K-REC was not easily observable in random conditions, because the K-shell of incident Xe^{53+} ions was rapidly filled up, mainly by nonradiative capture. Here we

use 60.1 MeV/u Kr^{36+} ions incident on a thin silicon crystal. The transmitted ions are still mostly bare in random as well as in channeling conditions, which allows to observe K-REC in both cases.

In section 2 we describe the experimental setup that allows charge state and energy analysis of the transmitted ions, and detection of photons coming from the impact area. In section 3 we present our experimental data, that include charge state distributions and high statistics X-ray energy spectra, and also an energy spectrum of photons detected in coincidence with well channeled ions. In section 4 we describe a simulation code that enables us to calculate both the amplitude and shape of the K-REC line. Compton profiles of silicon core electrons are calculated via a partial Fourier transform of the wave function as a function of the distance to the target atomic rows. Valence electrons are treated in a semi-classical way, as a non-uniform Fermi gas : electrons are considered as free electrons with exact solid state local densities. The confrontation of calculated and measured profiles is discussed in section 5. A fully exhaustive description of the K-REC line in terms of core and valence electron contributions is presented, and shows that silicon core electrons contribute still significantly in channeling conditions, and then should not be neglected as done in most channeling studies. We also show that the free electron model is a good approximation for valence electrons.

2 Experiment

The experiment was performed at GANIL (Caen, France), in the LISE beam line, designed for charge and energy analysis of highly stripped ions (fig. 1). The beam transverse emittance was given to be isotropic with 0.1 π *mm.mrad* (HWHM) projected along one direction, and the spot size on the target was at most equal to the spatial resolution of the multiwire chambers, which is 1 mm. Under these conditions, the beam intensity on the crystal was between 10 and 100 pA. The absolute number of incident ions was measured using a rotating beam chopper made of silver coated blades, from which the AgK_α X-rays were detected by a

Si(Li) diode. The crystal target was hold by a three-axis goniometer, which could be moved with an accuracy of 10^{-3} degree. The effective crystal thickness was $37\mu m$, a thickness that ensures single collision conditions for radiative capture by channeled ions, and charge state equilibrium for a random orientation, and allows energy loss measurements. Two intrinsic Ge detectors viewed the crystal, at 90° and 125°. Vertical slits were placed in front of the detectors, in order to limit Doppler broadening. A Si(Li) detector was set at 90°, but, as a lead shield masked the crystal target, it could view only the radiative decay of long lifetime excited states. Ions emerging from the crystal were magnetically charge- and energy-analyzed. A multiwire proportional gas counter placed in the dispersive focal plane was used to measure charge state fractions and energy losses. The resolution of this spectrometer was $\Delta p/p = 5.5\,10^{-4}$. Upstream from this wire chamber, two vertical slits could select ions of given energy and charge state. These ions were sent onto an Al foil, where they produced secondary electrons that were detected by means of a channeltron. This signal could be used as a trigger for the 90° Ge detector.

3 Results

In fig. 2 we present transmitted ion charge state distributions obtained with Kr^{36+}, Kr^{35+} and Kr^{33+} incident ions, respectively, under random and <110> alignment conditions. For random orientation the three distributions are found to be identical, which means that charge state equilibrium is reached within the $37\mu m$ thick Si target, in good agreement with theoretical predictions [13]. Most of the emergent particles are bare ions (74 %), which, as noted earlier, will allow to study K-REC by fully stripped ions in random conditions also. Nevertheless, since only bare and H-like ions can induce K-REC (with probabilities in a ratio of two to one), the K-REC cross section evaluation in random conditions will require the knowledge of the charge distribution averaged along the ion path in the target : for Kr^{36+} incident ions, the mean fraction values of Kr^{36+} and Kr^{35+} ions inside the target have been

calculated to be 77 % and 22 %, respectively.

In channeling conditions, fig. 2 shows that the charge distributions depend strongly on the incident charge state, which means that they are far from charge equilibrium. As Kr^{36+} and Kr^{35+} incident ions remain essentially frozen in their initial charge state, we are in a situation of single collision for both electron capture and loss. The electron capture probability is found to be about twice larger for bare ions than for H-like ions (4 % and 2.5 % respectively). As mechanical capture occurs preferentially in states with quantum number $n \geq 2$, and as K-REC is by far the dominant radiative capture process, such a result confirms that capture by channeled ions is dominated by K-REC. The probability of capturing two electrons successively is quite small, and is represented by the 34+ fraction obtained for Kr^{36+} incident ions (about 10^{-3}, with a large experimental uncertainty in this particular case). Channeled Kr^{35+} ions may lose their electron by EII since the K-shell binding energy is lower than the maximum energy transfer in an electron-electron collision at this beam velocity : it happens to about 9 % of them. For Kr^{33+} incident ions the charge distribution is dominated by EII, and only 40 % of them stay frozen in their initial charge state : their probability for losing one electron is dominated by the L-electron loss. Moreover, as the probability for losing successively three electrons is very small for channeled ions, the 36+ fraction (2 %) is fed essentially by the unchanneled part of the beam. As the 36+ fraction is largely dominant for random incidence, the above value of 2 % is equal to the unchanneled fraction (or more exactly to the fraction of ions able to lose electrons in close ion-atom collisions), which reflects very good channeling conditions.

Let us consider now the X-ray emission by channeled Kr ions, that gives a deeper insight into their interaction with the crystal electrons. X-ray spectra were recorded for various crystal orientations around the <110> direction.

In fig. 3 we present two energy spectra of photons detected at 90° from the Kr^{36+} beam direction, for random and <110> crystal orientation, respectively. They are normalized to

the same number of incident Kr^{36+} ions, corrected for dead time, and the background from surrounding radioactivity has been subtracted. First of all, channeling conditions are seen to cause a general reduction of the various components of the random spectrum, which is made of peaks due to the Kr Lyman series and to the radiative electron capture, and also of a continuum due to primary and secondary bremsstrahlung.

The Lyman lines are quite strongly attenuated (much more than REC lines) : the reason is that Lyman photons result mostly from deexcitation after non radiative capture into $(n > 1)$-shells or after excitation of a K-shell electron, both events taking place in close collisions with Si crystal atoms : the Ly_α yield is measured to be 2.5 % of the value obtained for random incidence, which is to be compared to the above 2 % fraction deduced from charge state measurements. In fact the Ly_α yield is slightly higher than 2 % because some channeled ions may contribute to this yield by deexcitation after L-REC capture.

In opposition with Lyman emission, bremsstrahlung and REC photons result basically from the interaction of the projectile with target electrons, and the photon yields depend on the mean electron density experienced by the projectile.

Primary bremsstrahlung is the photon emission by a target electron accelerated in the Coulomb field of the charged projectile. The maximum photon energy is equal to the kinetic energy E_c in the projectile frame of a target electron at rest in the laboratory frame. Secondary electron bremsstrahlung is a two-step process, in which a target electron is elastically scattered by the projectile, and then radiates part of its energy during slowing down in the target. The corresponding energy spectrum extends up to $\sim 4E_c$, since forward scattered electrons can be given twice the velocity of the projectile in the laboratory frame.

The attenuation of the bremsstrahlung yield in channeling conditions is measured to be 3.5, which corresponds to the ratio (14/4) of the total number of electrons per Si atom to the number of valence electrons.

The case of radiative electron capture is more interesting, and also more complex : not

only the K and L-REC peak integrals are lowered by channeling, but the line shapes are also strongly modified. In the following we will concentrate on the K-REC peak, that shows up the most distinctly against the continuum. It is clearly seen that for random crystal orientation the K-REC peak comprises broad wings that vanish almost completely in channeling conditions. For random incidence all types of target electrons may be captured, and the wings are due to the contribution of core electrons that present a broad Compton profile. In alignment conditions, channeled projectiles capture mainly valence electrons that present a much narrower Compton profile. Between these two extreme orientations (<110> axial channeling and random conditions) the body and wings of the K-REC peak evolve differently, as will be shown later. This means that a pertinent description of REC along the transition from channeling to random conditions requires a study of the peak shape, that reflects the various Compton profiles of the captured target electrons. Moreover, it has to be noted that not only the amplitude, but also the shape of the broad contribution due to the capture of core electrons varies from random to channeling conditions. Since the impact parameter distribution inside the crystal is quite different in each case, this suggests that the Compton profile of core electrons in a given atomic shell may depend on the location where the capture occurs.

In order to study more accurately radiative electron capture by channeled ions, we have performed a coincidence measurement using incident Kr^{36+} ions. The X-ray detector was triggered by the detection of a Kr ion transmitted with the charge 35+ (resulting from one electron capture), and with a reduced energy loss. We have selected channeled 35+ ions that have lost less than half of the random energy loss value. They represent 45 $\pm$ 7 % of the transmitted Kr^{35+} ions. The X-ray spectrum presented in fig. 4 (along with the corresponding single spectrum, similar to that already shown in fig. 3), is then uniquely due to channeled Kr ions that have captured one electron of the crystal by REC. Bremsstrahlung is largely washed out since only $\sim$ 2% of the total transmitted beam is selected for triggering the coincidence. The REC peaks appear nicely (including M-REC), as well as Ly_α, Ly_β and

Ly_γ lines that result from deexcitation after radiative electron capture into the L, M and N-shells, respectively. In particular L-REC and Ly_α peaks are found equal within 15 % (after correction for detector efficiency). The small discrepancy (in favor of L-REC) is probably due to slight differences in angular distributions of Ly_α and L-REC photons. The comparison of the coincidence spectrum with the corresponding single spectrum yields the most important feature related to the K-REC peak : the vanishing of the wings that are visible in the single spectrum, and that are due to the radiative capture of inner-shell target electrons by poorly or non channeled ions. The coincidence K-REC peak shows that well channeled ions can capture only electrons with a narrow Compton profile, i.e. valence electrons.

It is not easy to determine with precision the absolute mean energy of the K-REC peak : as the crystal was tilted by 35.2° when aligned along <110> direction, a small variation of the beam spot position on the crystal caused an significant shift of the K-REC peak, due to the Doppler effect. Nevertheless the comparison of the energies of K-REC peaks and Ly_α peaks (observed at 90° and 125°) indicates that, with respect to the theoretical energy (see below eq. (4)), there is no shift of the K-REC peak greater than 50 eV. We observe a significant variation of the mean energy of the K-REC peak between random and channeling conditions which can be explained (due to the drastic decrease of K-REC cross section with increasing photon energy) by the cumulated effects of the reduced energy loss and of the narrowing of the target electron Compton profile.

Moreover we have also obtained an X-ray spectrum (not shown) in coincidence with well channeled Kr^{34+} ions that have captured two electrons in the crystal. The 34+ fraction is very small for 36+ incident ions in channeling conditions (see fig. 2). We found no evidence for double K-REC (double electron capture accompanied by emission of one photon), which would correspond to photons around 94 keV at 90° in the laboratory frame. This was expected because the probability, for a channeled ion, to undergo a close interaction with two valence electrons simultaneously is quite low, much smaller than during binary collisions with atoms,

in which core electrons, more localized around the nucleus, can be captured.

At last, as mentioned above, we also recorded spectra of delayed X-rays with a Si-Li detector that could detect (at 90°) only photons emitted downstream from the crystal target. These spectra were obtained in coincidence with transmitted Kr^{35+} and Kr^{34+} well channeled ions. The results of this study of delayed photons are published separately [14]. They show that intrashell excitation plays a major rôle in the evolution of metastable states of the $n = 2$ levels in channeling conditions. A value of the cross section for 2s-2p mixing has been obtained.

4 Simulations

As noted above we have performed Monte Carlo simulations, in order to reproduce the experimental K-REC peaks. First we establish the ion flux in the crystal, i.e. the impact parameter distribution of moving ions with respect to atomic strings, and then their corresponding encounter probability. On the other side electron momentum distributions of target electrons to be captured are determined as a function of the impact parameter (i.e. of the place where the capture occurs). At last we discuss the K-REC cross sections that are needed to obtain absolute yields. Moreover the comparison with experimental data requires to substract the bremsstrahlung continuum, which is also discussed.

4.1 Distribution of transverse energy for channeled ions. Corresponding ion flux

An ion penetrating the crystal with an energy E is given a transverse energy $E_{T0} = E(\psi_0 + \delta\psi)^2 + V(\vec{r}_{0\perp})$ where ψ_0 is the mean angle between the beam direction and the crystallographic axis. $\vec{r}_{0\perp}$ and $\delta\psi$ are random variables which account respectively for the distribution of entrance positions (which is uniform), and entrance directions (which corresponds to the beam angular divergence around ψ_0). V is the continuum transverse potential.

It was calculated in ref. [9] in the case of the <110> axis of Si. Near the atomic strings, we have taken into account the influence on V of the thermal vibrations of the crystal atoms (1-D r.m.s thermal vibration amplitude at room temperature : $u_1 = 0.077$ Å) by using the single string potential proposed in ref. [15]. The beam angular divergence is supposed to be gaussian in any transverse direction. Various values of the angular width were considered in the simulations, in order to check the value given by the accelerator staff (HWHM of the angular spread projected along one direction : 0.1 mrad).

We assumed that statistical equilibrium is reached in the 4-D transverse phase space. As a consequence, a particle of given transverse energy E_T has a uniform probability to be at any point of the accessible transverse space, i.e. at any $\vec{r}_\perp$ where $V(\vec{r}_\perp) < E_T$ [16]. This is true only sufficiently far from the crystal entrance, since the incoming ions may keep a "phase memory" at the beginning of their path [17], over a characteristic path length Λ. In our case the crystal thickness ($t = 37\,\mu m$) is much greater than Λ ($\approx 2.5\,\mu m$) and one may consider that statistical equilibrium prevails all along the crystal.

In fig. 5 we present impact parameter distributions at statistical equilibrium $\Phi(b, \psi_0)$ inside the <110> crystal channel for various mean incidence angles ψ_0. Here we define the impact parameter as the distance b to the closest atomic string. $\Phi(b, \psi_0)$ is normalized as $\int \Phi(b, \psi_0)\ db = 1$. In the random incidence case, all positions in the transverse space are equiprobable. Then, for a single string (cylindrical geometry), the distribution $\Phi(b)$ increases linearly with b : $\Phi(b) = 2b/b_0^2$, $0 \leq b \leq b_0$, where b_0 is the radius of a unit cell in the transverse plane, associated to a single string ($\pi b_0^2 = 1/(Nd)$, where d is the interatomic distance along the <110> strings and N is the number of Si atoms per unit volume). The departure from this distribution above $b = 0.7$ Å is simply due to multistring effects.

In the same figure, we show first the distribution $\Phi(b, \psi_0 = 0)$ corresponding to an incident beam parallel to the <110> strings without any angular divergence. In this case the flux is strongly enhanced at large impact parameters, i.e. many ions are confined close to the

center of the channel (hyperchanneling). Conversely, small impact parameters are strongly inhibited : channeled ions cannot approach the target atom cores.

The drawback of using a quite thick crystal is that multiple scattering, which tends to increase the transverse energy of a particle, is not negligible. Both electronic and nuclear contributions (the latter being only significant for large E_T values) are taken into account in our calculations. Particles entering the target with a transverse energy E_{T0} suffer, when traversing the crystal, a mean transverse energy increase $\overline{\Delta E_T}$ induced by multiple scattering on target electrons and target nuclei. A good estimation of the contribution of target electrons to $\overline{\Delta E_T}$ can be obtained, following Bonderup et al. [18], from the mean energy loss of these particles through the crystal. For instance, for ions with very small E_{T0} values, we find $\overline{\Delta E_T}/Q = 6\ eV$ (where Q is the projectile charge). For the contribution of target nuclei, we used the treatment proposed in ref. [16] and developed in ref. [19]. The probability of REC events is small enough to ensure the validity of the hypothesis of the single collision regime ; consequently, the probability for a REC event to occur at given penetration depth z is uniform over $[0, t]$, where t is the target thickness. We have thus calculated the probability of a REC event for a particle entering the crystal with E_{T0} by considering that its transverse energy when the REC event may occur is $E_T = E_{T0} + \eta\overline{\Delta E_T}$, η being a random variable uniformly distributed over $[0, 1]$.

In fig. 5 we show a distribution $\Phi(b, \psi_0 = 0)$ for which a realistic beam angular divergence is taken into account : we assume an isotropic gaussian shape characterized by a width of 0.1 mrad HWHM when projected along one direction. Multiple scattering (before capture) is also taken into account in this calculation of $\Phi(b)$. Multiple scattering and incident beam angular divergence are seen to reduce hyperchanneling strongly. In the following, these effects will be included in the calculated distributions $\Phi(b)$ used in our simulations. We also show in fig. 5 the distribution $\Phi(b, \psi_0)$ corresponding to a beam entering the crystal with $\psi_0 = 0.03°$ (the relativistic Lindhard critical angle for channeling [16] is $\psi_c = 0.05°$ in our experimental

conditions). The distribution is very close to the one corresponding to the random case, except for small impact parameters $b \leq 0.2$ Å.

4.2 Electron densities in the channel

In order to simulate REC events, we have assumed that interactions with target electrons are binary events that can be considered independently. We have then to describe the interaction between an ion of well defined position $\vec{r}_\perp$ in the transverse plane and a target electron with a well defined wave function. The classical description of the ion trajectories is justified, owing to their high mass and velocity. In such a situation, REC yields could be calculated within the impulse approximation, following the treatment of ref. [12]. In fact we use here a simpler approach assuming that the probability for a REC event to occur at $\vec{r}_\perp$ is proportional to the mean electron density $\overline{\rho}(\vec{r}_\perp)$ at this point of the transverse space, i.e. averaged along the ion trajectory :

$$\overline{\rho}(\vec{r}_\perp) = \frac{1}{d}\int_{-d/2}^{d/2} \rho(\vec{r}_\perp, z)\, dz \qquad (1)$$

where d is the interatomic distance along the <110> string. In fact, such an hypothesis is supported by comparing the dependence of REC probability with impact parameter calculated in ref. [12] for target Si electrons in various initial atomic quantum states (nlm) captured by high velocity Xe ions to the mean corresponding electronic density $\bar{\rho}_{nlm}(\vec{r}_\perp)$. The comparison is shown in fig. 6 for the capture of L shell Si electrons. In fact, taking into account the axial symmetry around a string, we compare $bP_{K-REC}(b)$ to $b\overline{\rho}_L(b)$ ($\overline{\rho}_L(b) = \overline{\rho}_{2s}(b) + \overline{\rho}_{2p}(b)$). The shapes are nearly identical ; the only difference consists in a small shift $\delta b = 0.03$ Å on the abscissa of the two curves. This shift is small when compared both to the extension of $b\overline{\rho}_L(b)$ and to the uncertainty on the impact parameter dependence of the channeled ion fluxes. We thus decided to neglect it.

The electron encounter probability of incident projectiles depends on the flux distribution $\Phi(b, \psi_0)$ and on the densities $\bar{\rho}_{st}(b)$ associated to given electronic states of silicon

$(1s, 2s, 2p$,valence) averaged over z. In fig. 7 we show the mean electron encounter probability $g(b, \psi_0)$, together with the various $\bar{\rho}_{st}(b)$, as a function of impact parameter b. The $g(b, \psi_0)$ values are obtained from products $\bar{\rho}(\vec{r}_\perp)\Phi(\vec{r}_\perp, \psi_0)$ in the Monte-Carlo calculations, $\bar{\rho}(\vec{r}_\perp)$ being the total mean electronic density for $\vec{r}_\perp$. The three distributions $g(b)$ shown correspond to the three incident beam orientations (random, $\psi_0 = 0$ and $\psi_0 = 0.03°$) already considered in fig. 5. For the random orientation, $g(b)$ is simply proportional to $\bar{\rho}(b)$. The densities $\bar{\rho}_{st}(b)$ were calculated from the atomic wave functions of ref. [20] in the case of core electrons and, for valence electrons, using the Fourier coefficient of ref. [21] obtained with nonlocal pseudo-potentials.

The analysis of fig. 7 provides information on the contribution to $g(b, \psi_0)$ of each electronic state. For $\psi_0 = 0$, the capture of valence electrons takes place preferentially at large distance from the target strings : more electrons are captured at $b > 0.8$ Å than in the random case. However, the overall valence capture yield, i.e. the integral over b of the valence encounter probability, is lower than in the random case, for which the encounter can also occur at smaller b, i.e. in regions of higher valence electron densities. This is illustrated by the map of fig. 8, which shows that the valence electron density is maximum between the closest strings : these electrons are the binding electrons of the crystal lattice. They cannot be captured by well channeled ions since the potential in this region is rather high (around 19 eV per unit charge), although much smaller than the critical transverse energy E_{TC} ($E_{TC}/Q = E\psi_c^2/Q \simeq V(b \simeq 0.15$ Å$)/Q = 110\, eV$). As a consequence, the overall valence electron encounter probability is smaller than in the random case only for tilt angles ψ_0 significantly smaller than ψ_c. One can see in fig. 7 that, already for a tilt angle $\psi_0 = 0.03° = 0.6\psi_c$, there is no more effect.

Since small impact parameters are forbidden for channeled ions, their encounter probability with core $2s$ and $2p$ electrons which are rather localized near the nuclei is much smaller than in the random case. As the spatial extension of $\rho_{nlm}(b)$ is quite similar for these two states, the corresponding encounter probabilities are reduced by about the same amount in

channeling. Of course the smaller the impact parameter the stronger this reduction. The reduction of the $1s$ electrons contribution is still stronger. At the intermediate tilt angle ($\psi_0 = 0.03°$), the encounter probability with $2s$ and $2p$ electrons increases markedly but is still much smaller than in the random case (note that $1s$ electrons are still almost entirely hidden). It must be pointed out that not only the overall encounter probability but also the variation of the local encounter probability with impact parameter depend strongly on ψ_0.

4.3 Momentum distribution of target electrons at a given impact parameter

The shape of the measured REC lines is mainly determined by the momentum distribution of the captured electrons. A calculation of this distribution requires the knowledge of the target electrons wave functions. We have considered separately the contribution of core and valence electrons. In sect. 4.2 we have shown (see fig. 6) that REC events take place at given $\vec{r}_\perp$ with a probability proportional to $\bar{\rho}(\vec{r}_\perp)$. We shall now assume that the shape of the REC peak of capture events taking place at $\vec{r}_\perp$ depends on the momentum distribution of the electrons at this point of the transverse space. For this purpose, we have used the electronic wave functions in a mixed representation $\Psi(\vec{r}_\perp, p_z) = \Psi(b, p_z)$ (we recall that b is the distance to the closest string for a particle at $\vec{r}_\perp$). We thus calculate the partial Fourier transform :

$$\Psi_{n\ell m}(b, p_z) = \frac{1}{\sqrt{2\pi\hbar}} \int_{-\infty}^{+\infty} \phi_{nl}\,(\sqrt{b^2 + z^2}) Y_{\ell m}(\theta)\, e^{\frac{ip_z z}{\hbar}}\, dz \qquad (2)$$

where $tg\theta = b/z$, ϕ_{nl} is the radial atomic wave function and Y_{lm} its angular part.

The probability density $|\Psi_{n\ell m}(b, p_z)|^2$ is the conditional momentum distribution $J_{nlm}(p_z \mid b) = J_{nl}(p_z \mid b)$ of a core electron at given b. This distribution is normalized through :

$$\int_0^{+\infty} 2\pi b\, db \int_{-\infty}^{+\infty} |\Psi_{n\ell m}(b, p_z)|^2 dp_z = 1 \qquad (3)$$

From $J_{nl}(p_z \mid b)$ one may easily deduce the momentum distribution $J_{nl}(p_z \mid \vec{r}_\perp)$ in the channel. In our simulations we have determined the momentum distributions $F_{nl}(p_z, \psi_0)$ of electrons

of a given state captured by incident ions, when the beam enters the crystal with an incident angle ψ_0. Such a distribution is obtained by averaging the distributions $J_{nl}(p_z \mid \vec{r}_\perp)$ with a weight $g_{nl}(\vec{r}_\perp, \psi_0) = \rho_{nl}(\vec{r}_\perp)\Phi(\vec{r}_\perp, \psi_0)$ (note that for random incidence, $\Phi(\vec{r}_\perp, \psi_0 \gg \psi_c)$ is constant).

In fig. 9 we present the shapes of $F_{nl}(p_z, \psi_0)$ corresponding to $2s$ and $2p$ electrons for various ψ_0 values. The calculations were performed as in fig. 7 for $\psi_0 = 0$, $\psi_0 = 0.03°$ and $\psi_0 \gg \psi_c$ (random). For convenience, the momentum values in abscissa are converted in REC photon energy dispersion in the projectile frame (the p_z are multiplied by $\beta\gamma c$, see eq. (4) below). For an easier comparison of shapes, the profiles are represented with the same maximum amplitude. There is a clear dependence on ψ_0 of the shape of the distributions corresponding to $2p$ electrons, which provide the major contribution to the total core Compton profile. Such an effect is much weaker on the distributions corresponding to $2s$ electrons. The general trend is that the momentum distribution of captured electrons is narrower in aligned than in random condition. As the ion flux distribution for an aligned beam favors large b values, the effect observed can be understood in a classical picture, considering that target electrons of given state have a lower mean kinetic energy at large b, where the potential energy is higher.

For $1s$ electrons of silicon, the spatial extension of the wave function is of the same order than the target atoms thermal vibrations. Thus, even for a beam entering the crystal parallel to the <110> rows, the particles which can capture $1s$ electrons are those which approach very close to the strings. They experience strong multiple scattering, and they can rapidly be considered as unchanneled particles which sample uniformly the crystal. Then we directly used the atomic Compton profile of $1s$ silicon electrons tabulated in ref. [22], which is already averaged over b.

In principle, the calculation of the Compton profile associated to the capture of valence electrons should be performed in a similar way than for L silicon electrons. Unfortunately, we

are dealing with an extremely large number of wave functions (Bloch waves). Moreover, these Bloch waves are obtained as linear combinations of plane waves ; thus, Fourier transformation (eq. (2)) raises very severe computational problems, related to the fact that the Fourier transform of a plane wave is a Dirac distribution. We then decided to use a semi-classical treatment based on a description of valence electrons as a non uniform free electron gas. In such a description, the only relevant parameters are the density $\rho(\vec{r}_\perp, z)$ and the associated momentum distribution $J_F(p_z \mid \vec{r}_\perp, z) = \frac{1}{2} p_F(\vec{r}_\perp, z)$ with $-p_F(\vec{r}_\perp, z) \leq p_z \leq p_F(\vec{r}_\perp, z)$ and where $p_F(\vec{r}_\perp, z) = \hbar(3\pi^2 \rho(\vec{r}_\perp, z))^{1/3}$ is the Fermi momentum experienced by an ion along its trajectory. The density $\rho(\vec{r}_\perp, z)$ to be considered to calculate p_F is the total electron density $\rho_{val}(\vec{r}_\perp, z) + \rho_{core}(\vec{r}_\perp, z)$: a valence electron captured in regions where the core electron density ρ_{core} is significant has a momentum distribution which is broadened by these core electrons. Calculating the shape of the Compton profile associated to the capture of valence electrons within the frame of this semi-classical treatment is questionable ; however, in aligned geometry, valence electrons are mostly captured in region where ρ_{core} is negligible and $\rho(\vec{r}_\perp, z)$ varies rather smoothly with the coordinates, and it seems appropriate to use a free electron gas model. An interesting feature of the results of ref. [12] is, as stated in sect. 4.2, that the range of the interactions leading to a REC event is very limited (a capture in $\vec{r}_\perp$ has a probability proportional to $\overline{\rho}(\vec{r}_\perp)$ to occur, see fig. 6). In our semi-classical treatment, it is thus natural to assume that REC is a local process, taking place at a well defined coordinate $(\vec{r}_\perp, z)$ with a probability proportional to $\rho(\vec{r}_\perp, z)$ and that the momentum distribution of the electron captured at this point is given by $J_F(p_z \mid \vec{r}_\perp, z)$.

We have checked the validity of the semi-classical treatment by applying it both to core and valence Si electrons, such a treatment being indeed much more doubtful for the former than for the latter. In this way we obtained Compton profiles $C_{p1}(p_z \mid b)$ calculated by averaging $J_F(p_z \mid \vec{r}_\perp, z)$ over z with the weight $\rho(\vec{r}_\perp, z)$. They are compared in fig. 10 to profiles $C_{p2}(p_z \mid b)$ calculated by the quantum treatment through eq. (2) for core electrons and semi-classically for valence electrons by averaging $J_F(p_z \mid \vec{r}_\perp, z)$ over z with the weight

$\rho_{val}(\vec{r}_\perp, z)$. As in fig. 9 the scaling factor $\beta\gamma c$ is used for p_z. At low impact parameters ($b \leq 0.3$ Å) i.e. in regions of high and strongly b-dependent electronic densities, the profiles $C_{p1}(p_z \mid b)$ are markedly too broad and thus the semi-classical treatment is not appropriate. On the contrary, the agreement between the widths of $C_{p1}(p_z \mid b)$ and $C_{p2}(p_z \mid b)$ is fair for $b \geq 0.3$ Å (the discrepancy never exceeds 10%). However, a significant difference remains for large p_z values : the semi-classical treatment does not reproduce the wings predicted by the quantum treatment. Still, the comparison of $C_{p1}(p_z \mid b)$ and $C_{p2}(p_z \mid b)$ demonstrates that the semi-classical treatment applied to all target electrons provides already rather correct Compton profiles in regions where the overall electron density is not too high. It can thus be applied with confidence to the valence gas, for which, as indicated above, a full quantum treatment is out of reach.

The momentum distributions of valence electrons at point $\vec{r}_\perp$ $C_{p1-val}(p_z \mid \vec{r}_\perp)$ obtained from the semi-classical treatment can be averaged over $\vec{r}_\perp$, leading to the distribution $F_{val}(p_z)$. If we attribute to each position $\vec{r}_\perp$ a weight proportional to $\bar{\rho}_{val}(\vec{r}_\perp)$, we simulate the Compton profile $F_{val-rand}(p_z)$ associated to a uniform ion flux in the crystal (random situation). Such a profile can be compared to the experimental determination performed in high resolution X-ray measurements [23]. The comparison is shown in fig. 11. The agreement is satisfactory and confirms again the validity of the semi-classical approach that we have used.

4.4 Intensity and shape of the REC peak

After obtaining the longitudinal target electron momentum distribution, we determined the K-REC peak shape according to the following procedure. In the projectile frame, the relation between the energy $h\nu$ of the K-REC photon and the captured target electron momentum for a given position $\vec{r}_\perp$ in the channel is :

$$h\nu = E_c + E_K - \gamma E_i - \beta\gamma c p_z \tag{4}$$

where E_K and E_i are respectively the final and initial binding energies of the electron, γ the Lorentz factor and $E_c = (\gamma - 1)m_e c^2$ is the kinetic energy of an electron with the ion velocity v_{ion}.

We calculated the K-REC capture probability within the impulse approximation. We used the non relativistic dipole approximation [24]. For the radiative recombination of a free electron in the ion K shell, the cross section is :

$$\sigma_{K-REC} = \frac{2^7\pi}{3} \frac{e^2}{m_e c^2} \frac{h}{m_e c} \frac{E_K^3}{h^2\nu^2(h\nu - E_K)} \exp(-\frac{4\zeta \tan^{-1}(1/\zeta)}{1 - \exp(-2\pi\zeta)}) \quad (5)$$

where $\zeta = \sqrt{E_K/(h\nu - E_K)}$. In our experiment, the captured electrons are initially bound. As these binding energies are significantly smaller than E_c, we decided however to use eq. (5). In this equation, σ_{K-REC} can be considered as a function of the photon energy $h\nu$. As seen in eq. (4), $h\nu$ depends both on the initial binding energy and momentum of the electron. The influence of the initial state on σ_{K-REC} was thus taken into account through these dependences.

$h\nu$ depends also (and mainly) on the ion kinetic energy E_c. This energy decreases quasi-linearly inside the target. In order to fit the experimental K-REC peak we have thus taken into account in the calculations the mean energy loss $\overline{\Delta E}$ of the projectile inside the crystal, which differs from channeling to random conditions. As a REC event can take place at any penetration depth, this induces a decrease $-(m_e/M_{ion})\ \Delta E$ of $h\nu$ in expression (4), ranging quasi-uniformly from zero to $-(m_e/M_{ion})\ \overline{\Delta E}$.

The REC peak was determined in the ion frame by a Monte-Carlo simulation in the following way. For an incident ion indexed by i, a transverse energy E_{iT} is chosen, according to the distribution of incident impact parameters and angles, and according to the mean transverse energy increase induced by multiple scattering, ΔE_T. Then a $\vec{r}_{i\perp}$ position is sampled uniformly in the accessible transverse space. At this position an electron momentum p_z is chosen according to the corresponding distribution. For p_z, the distribution can correspond either to core or valence electrons with weights proportional to $\bar{\rho}_{core}(\vec{r}_{i\perp})$ and $\bar{\rho}_{val}(\vec{r}_{i\perp})$ respec-

tively. We then calculated, via eqs. (4) and (5), the photon energy $h\nu_i$ and the probability $P_i = \sigma_{K-REC}\ \overline{\rho}(\vec{r}_{i\perp})t$ (where t is the target thickness) for a K-REC event to occur. This procedure was iterated : the P_i values added at the corresponding abscissa $h\nu_i$ give the REC peak.

This calculation can be performed for any beam entrance conditions. It has been applied to various mean entrance angles ψ_0 with respect to the <110> rows. It has also been used at random incidence case for which all incident particles sample uniformly the whole transverse plane.

In order to simulate our experimental results, we have to determine the shape and intensity of the REC peak in the laboratory frame from the calculation performed above in the ion rest frame. We must then perform the Lorentz transform of the photon peak. We assumed a $sin^2\theta_{lab}$ dependence of the angular distribution of the K-REC photons [25]. We also convoluted the photon peak with a distribution function resulting from the measured detector resolution and Doppler broadening associated to the detector collimator aperture. The combined contribution to the K-REC peak width of ion energy loss inside the crystal, Doppler effect and detector resolution, is quite small compared to the width of the Compton profile : for the valence electrons contribution (i.e. with smallest momenta), the Compton profile width is still 3 times larger. Higher order REC (L-, M-REC) lines were obtained in the same way than the K-REC line. The relative normalization factors of L- and M-REC with respect to K-REC were deduced from the coincidence spectrum of fig. 4, where the various contributions are resolved without any background. We did not distinguish between the radiative capture into the separate $2s$, $2p_{1/2}$ and $2p_{3/2}$ sublevels ; this separation causes an additional broadening ($\sim 80\ eV$) of the L-REC that is much smaller than the Compton profile, and then negligible.

4.5 Calculation of the background induced by bremsstrahlung

In order to estimate with precision the background below the REC peaks to be subtracted, we have calculated for each spectrum the shape of the bremsstrahlung contribution. The primary bremsstrahlung (bremsstrahlung of a target electron in the field of the bare projectile) is obtained within the Sommerfeld-Maüe method (distorted wave-unscreened potential [26]). Then the theoretical profile is convoluted with the silicon Compton profile, which depends on the crystal orientation. The secondary electron bremsstrahlung is calculated as in ref. [27] by applying the Mc Kinley-Fesbach equation for elastic scattering and the treatment of Koch and Motz [28] on electron bremsstrahlung to atomic silicon. Using these calculations to adjust our experimental background is questionable for three reasons : *i)* in the calculation, all secondary electrons are assumed to stop inside the crystal. In fact the range of a "knock-on" electron with highest energy $E_{max} = 2\gamma^2\beta^2 m_e c^2 = 136\ keV$ is about 300 μm in silicon [29], which is much larger than our crystal thickness. *ii)* In the calculations, the secondary electron bremsstrahlung emission is assumed to be isotropic. This is doubtful, particularly for hard photons which are emitted by energetic binary electrons, i.e. electrons scattered in the forward direction. *iii)* The bremsstrahlung yield depends strongly on ion channeling effects (see sect. 3). However as one observes that the calculations reproduce quite well the shape of the experimental background, we have decided to set primary and secondary electron bremsstrahlung amplitudes as free parameters in the fits of the spectra and to keep the calculated shape. For random spectra, typical multiplying factors used to adjust the calculations to the experimental background are in the range 0.8 to 1.5.

5 Comparison to experiments

5.1 Fitting the X-ray spectra

In fig. 12 we compare experimental and simulated X-ray spectra in the case of random and <110> aligned geometries. For the simulations, the contributions of primary and secondary electron bremsstrahlung and the contributions of core and valence electrons to the REC peaks are indicated separately. The respective weights of all these contributions were adjusted in order to obtain the best fit : here, the simulations are only used to predict shapes. The random spectrum calculated this way is seen not to fit perfectly the experimental spectrum on the high energy side of the K-REC peak, corresponding to the capture of electrons with high initial momentum. This discrepancy is not related to the uncertainty on the calculated contribution of secondary bremsstrahlung, since this contribution is quite small in this region. Most probably, the use of the impulse approximation in eqs. (4) and (5) is no longer valid when the binding energy of the electron to be captured becomes non negligible as compared to its kinetic energy viewed from the projectile frame, and thus the wings of the REC peaks are not perfectly estimated. Except for this small discrepancy, the agreement between simulations and experiments in both spectra of fig. 12 is remarkable.

5.2 Fitting the REC yield dips

As mentioned in sect. 3, we estimated, for each beam incidence angle ψ_0, the mean fraction of ions that capture mechanically one or more electrons inside the target. For Kr^{35+} ions we assigned a K-REC probability divided by 2 ; of course, for lower charge states, there is no K-REC. In fig. 13 we show the comparison of experimental and calculated K-REC dips, corresponding to the capture of valence electrons (fig. 13-a) and of core electrons (fig. 13-b). All the dips are normalized with respect to the random REC yield, measured or calculated for $\psi_0 \gg \psi_c$. The experimental dips were obtained from the best fits of the spectra as shown in fig. 12, i.e. by adjusting each contribution to the REC peak. Here the error bars are due

to the uncertainties in the fit (subtraction of bremsstrahlung, partition between core and valence contributions when both are large), and to the uncertainty in the evaluation of the corrective term for the fraction of ions with one or more electrons inside the crystal. The calculated dips were obtained from the simulations, as described in sect. 4.4. Simulations were performed assuming an isotropic gaussian beam angular divergence with various widths. The best agreement, both for the dips corresponding to valence and core electrons, is obtained for a value of 0.1 mrad HWHM projected along one direction, in good agreement with the value given by the accelerator staff.

Concerning the behavior of the valence electron contribution, the experiments and the calculations are in good agreement and show unambiguously the existence of a narrow dip. The uncertainty on the fit is here negligible since both bremsstrahlung background and core electron contribution to K-REC are very small close to the <110> orientation. The agreement is also very good for the core electron contribution. The value of the calculated minimum yield ($\chi_{core} = 0.055$, with a 10% uncertainty due to the statistics of the simulations) reproduces correctly the measured ratio between axial and random orientation : $\chi_{core} = 0.060 \pm 0.017$. Although strongly attenuated in alignment conditions, the core electron contribution to the total K-REC yield is found to be 15%, which is not negligible.

The shoulder effect observed on the experimental dip around $\psi_0 = 0.06°$, i.e. for entrance angles slightly greater than ψ_c, cannot be predicted by our simulations. The latter are based on rather simple approximations to describe channeling effects (see 4.1). In particular we assume that : *i)* particle trajectories are determined by a continuum axial potential, *ii)* the ion flux distributions correspond to statistical equilibrium and *iii)* all entrance directions with given ψ_0 are equivalent i.e. that planar channeling effects can be neglected. These three hypotheses, that are valid for $\psi_0 \leq \psi_c$, do not allow to reproduce experimental shoulder effects that depend markedly on the scanning direction. One important result of fig. 13-b is that χ_{core} is significantly higher than the value $\chi_{\min} = 0.025$, measured for Ly_α emission

for instance. This is due to the fact that the density associated to $2s$ and $2p$ Si electrons is significant even at distances of $\simeq$ 0.3 Å from the nuclei (see fig. 7), which are much larger than the r.m.s amplitude of thermal vibrations. As a consequence, core electrons contribute to $\simeq$ 13% of the total K-REC yield when the beam enters along the <110> direction.

5.3 Determination of the K-REC cross section

The K-REC cross section can be extracted from the absolute yield values measured for random orientation (figs. 13-a and 13-b). They are found to be nearly identical and close to the prediction of the nonrelativistic dipole approximation ($\sigma_{K-REC} = 39 \times 10^{-24}\ cm^2$) : the cross sections per target electron obtained from the valence and from the core electrons contribution are respectively : $\sigma_{K-REC} = (38.5 \pm 1.2 \pm 5.8)10^{-24}\ cm^2$ and $\sigma_{K-REC} = (42.9 \pm 2.4 \pm 6.4)10^{-24}\ cm^2$. The first uncertainty corresponds to the error bars in fig. 13, and is thus related to the fitting procedure. The second one is our experimental absolute uncertainty (15 %).

It is of interest to compare the σ_{K-REC} values that we obtain to the compilation of experimental cross sections presented in ref. [30], where cross sections are compared to the prediction of the non relativistic dipole approximation for a large variation range of the adiabaticity parameter $\eta = \frac{1}{\zeta^2} = \frac{E_{ion}}{Z^2 E_{Bohr}} \frac{m_e}{M_{ion}}$ where $E_{Bohr} = 13.6\,eV$. Most of the results correspond to experiments performed with gas targets, and very often the measured values are systematically $\approx$ 30% lower than the theoretical predictions. However, for η values in the 1-3 range, which corresponds to our experimental situation ($\eta = 1.86$), the compiled data are in good agreement with the predictions. Also, in this η range, no difference is observe between cross sections measured for gas and solid targets. In a paper devoted to the study of REC by channeling, the authors of ref. [3] have assumed, in order to interpret their results, that the REC yield for ions travelling into solids could be strongly enhanced by the so-called "wake effect" which modifies the electron density and momentum distribution around the

ion. In fact their conclusions on REC cross sections rely on an estimate of the mean electron density that is quite questionable (they consider that the whole ion flux in <110> alignment conditions is strictly restricted within the central region of the channels. This is erroneous, since it is clear that even with a perfect beam, the particle flux extends to the whole transverse space, although in a non uniform way, cf. our section 4.1). It is nevertheless worthwhile to discuss the influence of the wake effect on REC, that, according to Pitarke et al.[31], should in principle affect the REC yield and also the shape and energy position of the REC lines. These authors show that the amplitude of the response of the target electrons to the ion passage scales as $\zeta = \eta^{-\frac{1}{2}}$, which should affect REC yields significantly for ζ values above unity. In our case, $\zeta = 0.73$ and the wake effects on the yield should be quite small.

Concerning the position of the REC peak, the wake effect shift predicted by Pitarke et al. [31] should be around $20\,eV$, i.e. a value too small to be evaluated owing to our experimental precision. The REC yield is proportional, in a first approximation, to the electron density ρ^* around the ions, which should depend on the wake effect. The dependence of the *K-REC* peak width with ρ^* is weaker : in the simple case of a Fermi gas, this dependence scales as $(\rho^*)^{\frac{1}{3}}$. As indicated above, in the η range corresponding to our experiment, neither the results obtained on gas targets nor those corresponding to solid targets (i.e. our measurements, but also experiments performed with 295 MeV/u uranium ions on beryllium and carbon [30]) show any significant departure from the predicted cross sections. As, moreover, we find a good agreement between calculated and measured line shapes (see fig. 12), we conclude that for $\zeta < 1$ (i.e. $\eta > 1$), wake effects have a negligible influence on REC.

5.4 K-REC of valence electrons

The coincidence spectrum shown in fig. 4 is associated to the X-ray emission induced by the 45% ions having suffered the smallest energy losses (see sect. 3). Assuming to a first order a biunivocal relationship between the energy loss and the transverse energy of an

ion, i.e. neglecting energy loss fluctuations, one can consider that these ions are the best channeled ones, with a well defined upper limit in transverse energy $(E_T/Q)_{\max}$. The K-REC peak observed (that we will call $S_{\exp}$) corresponds thus essentially to the capture of target valence electrons. In fig. 14-a we compare $S_{\exp}$ to the K-REC peak (S_{calc}) calculated using the experimental Compton profile of Si valence electrons determined in ref. [23] and taking for the K-REC cross section the value $\sigma_{K-REC} = 38.5 \times 10^{-24}\ cm^2$ that we have experimentally determined. In fig. 14-a, the integral of S_{calc} was adjusted to the one of $S_{\exp}$, using a normalizing factor $\kappa = 0.56$. S_{calc} corresponds to the valence contribution to K-REC for the whole incident beam at random incidence. As $S_{\exp}$ arises from an aligned incident beam and corresponds to a selection of part of this beam, it is natural to expect differences both in the integral (this explains why κ had to be introduced) and in the shape of $S_{\exp}$ and S_{calc}. In fact, one can observe in fig. 14-a that $S_{\exp}$ and S_{calc} have quite comparable shapes. However, the FWHM of $S_{\exp}$ is slightly narrower, $1.64 \pm 0.05\ keV$ against $1.8\ keV$ for S_{calc}. As this width is related to the electron density of the captured electrons, this result demonstrates that the ions selected in the coincidence experiment sample valence electron densities hardly smaller than those sampled by a uniform ion flux.

We have used our Monte-Carlo simulations in order to determine the characteristics of the channeled ions selected in the coincidence experiment. As shown in sect. 4.3, the simulations provide in particular the location $(\vec{r}_{i\perp}, z_i)$ at which an ion with transverse energy E_{iT}, leaving the crystal with a charge state 35+, has suffered a K-REC event. One can then determine to what fraction of the incident beam correspond the 45% best channeled ions with 35+ outgoing charge state which were selected, and which electron densities they sampled. From our simulations (where we determine a cut-off in transverse energy in order to adjust the S_{calc} integral to S_{exp}), we find that the selected ions originate from 65% of the incident beam, with a cut-off $(E_T/Q)_{\max} = 16\ eV$. As the $V(\vec{r}_\perp)/Q$ value is around 19 eV in regions where the valence electron density is maximum, i.e. close to the cut-off value, we conclude that many of the selected ions may sample regions of high ρ_{val}. The simulations provide

mean values of explored electron densities : $< \bar{\rho}_{val} >_i = (1/n) \sum_{i=1}^{i=n} \bar{\rho}_{val}(\vec{r}_{i\perp}) = 0.157$ Å^{-3} and $< \rho_{val} >_i = (1/n) \sum_{i=1}^{i=n} \rho_{val}(\vec{r}_{i\perp}, z_i) = 0.223$ Å^{-3}. These mean values are slightly smaller than the one sampled by a uniform flux, which are respectively equal to 0.2 Å^{-3} (4 valence electrons per Si atom) and 0.255 Å^{-3}. This is consistent with the fact that $S_{\rm exp}$ is slightly narrower than S_{calc} in fig. 14-a. It is also consistent with the fact that the normalizing factor $\kappa = 0.56$ applied to S_{calc} is slightly smaller than the value 0.65 which corresponds to the fraction of the incident beam which was selected. Another conclusion of the simulation is that 97.5% of the selected ions have captured a valence electron and only 2.5% have captured a core electron.

In fig. 14-b, we compare S_{exp} to the K-REC peak S_{sim} obtained from the simulation (see sect. 4.3). Let us recall that this calculation relies on a rather crude description of the valence electron momentum distribution. However, S_{sim} reproduces surprisingly well the shape of S_{exp}. In particular the full width at half maximum of S_{sim} (1.61 keV) is found to be in good agreement with the experimental value (1.64 keV). There is still a small discrepancy in the wings corresponding to high longitudinal electron momenta, which are underestimated in S_{sim}. This discrepancy sets the limits of the free electron model that we have used.

6 Summary and conclusion

We have measured K-REC by channeled and unchanneled bare krypton ions in a thin silicon crystal. We have analyzed in details the contribution of each electronic subshells of the target atoms. A complete decomposition of the K-REC peak has been obtained with the help of simulations which calculate the momentum distribution of captured valence, $2s$ and $2p$ electrons of silicon (the latter L-shell electrons contribute significantly - by 15% - to the REC peak in channeling conditions). The comparison between experiments and simulations provide information on the dependence of the electron momentum distributions with the position $\vec{r}_\perp$ in the transverse plane perpendicular to the <110> strings. This dependence is

strong both for valence and $2p$ electrons. The K-REC cross section is found very close to the value obtained from the non relativistic dipole approximation calculation. We thus conclude that, for the value of the adiabaticity parameter η corresponding to our experiment, wake effects have a small influence on REC.

Beam angular divergence and multiple scattering of ions inside the quite thick crystal did not enable us to perform a specific study of hyperchanneled ions, i.e. ions which explore only regions in the transverse space very far from the atomic rows where valence electron Compton profiles are expected to be very narrow. However, we have measured K-REC peak corresponding to the capture of valence electrons by the best channeled ions selected through their energy loss. This peak is well reproduced by simulations in which the valence electrons are described in the frame of a non uniform Fermi gas model.

We would like to thank J. Moulin and the CIRIL staff for their technical help, Y. Bernard for his help in X-ray topography measurements performed to check the crystal quality, and the GANIL accelerator crew for delivering us an ion beam of high quality. We thank also J.E. Miraglia, R. Gayet and A. Salin for providing us the results of their calculations. The supports of NATO under research grant CRG890597 and of the French CNRS under GDR 86 are gratefully acknowledged.

References

[1] B.R. Appleton, R.H. Ritchie, J.A. Biggersaff, T.S. Noggle, S. Datz, C.D. Moak, H. Verbeek and V.N. Neelavathi, Phys.Rev. **B19**(1979) 4347.

[2] S. Andriamonje, M .Chevallier, C. Cohen, J. Dural, M.J. Gaillard, R. Genre, M. Hage-Ali, R. Kirsch, A. l'Hoir, B. Mazuy, J. Mory, J. Moulin, J.C. Poizat, Y. Quéré, J. Remillieux, D. Schmaus and M. Toulemonde, Phys.Rev.Lett. **59** (1987) 2271.

[3] L.C. Tribedi, V. Nanal, M.B. Kurup, K.G. Prasad and P.N. Tandon, Phys. Rev. **A51**(1995)1312

[4] S. Datz, C.R. Vane, P.F. Dittner, J.P. Giese, J. Gomez del Campo, N.L. Jones, H.F. Krause, P.D. Miller, M.Schulz, H. Schöne and T.M. Rosseel, Phys.Rev.Lett. **63** (1989) 742.

[5] A. Belkacem, E.P. Kanter, K.E. Rehm, E.M. Bernstein, M.W. Clark, S.M. Ferguson, J.A. Tanis, K.H. Berkner and D. Schneider, Phys.Rev.Lett. **64** (1990) 380.

[6] S. Andriamonje, M. Chevallier, C. Cohen, N. Cue, D. Dauvergne, J. Dural, R. Genre, Y. Girard, R. Kirsch, A. L'Hoir, J.C. Poizat, Y. Quéré, J. Remillieux, D. Schmaus and M. Toulemonde, Phys.Lett. **A164** (1992) 184.

[7] J.U. Andersen, J. Chevallier, G.C. Ball, W.G. Davies, J.S. Forster, J.S. Geiger, J.A. Davies and H. Geissel, Phys.Rev.Lett.**70** (1993) 750.

[8] N. Claytor, B. Feinberg, H. Gould, C.E. Bemis, J. Gomez del Campo, C.A Ludemann and C.R. Vane, Phys.Rev.Lett.**61** (1988) 2081.

[9] A. L'Hoir, S. Andriamonje, R. Anne, N.V. De Castro Faria, M. Chevallier, C. Cohen, J. Dural, M.J. Gaillard, R. Genre, M. Hage-Ali, R. Kirsch, B. Farizon-Mazuy, J. Mory, J. Moulin, J.C. Poizat, Y. Quéré, J. Remillieux, D. Schmaus and M. Toulemonde, Nucl.Instr. and Meth. **B48** (1990) 45.

[10] S. Andriamonje, R. Anne, N.V. De Castro Faria, M. Chevallier, C. Cohen, J. Dural, M.J. Gaillard, R. Genre, M. Hage-Ali, R. Kirsch, A. L'Hoir, B. Farizon-Mazuy, J. Mory, J. Moulin, J.C. Poizat, Y. Quéré, J. Remillieux, D. Schmaus and M. Toulemonde, Phys.Rev.Lett. **63**(1989) 1930.

[11] P.F. Dittner, C.R. Vane, H.F. Krause, J. Gomez del Campo, N.L. Jones, P. Zeijlmans van Emmichoven, U. Bechtold and S. Datz, Phys.Rev. **A45** (1992) 2935.

[12] J.E. Miraglia, R. Gayet and A. Salin, Europhys.Lett.**6** (1988) 397 and private communication for calculations on xenon.

[13] J.P. Rozet, C. Stephan and D. Vernhet, to be published in Nucl.Inst.Meth.**B.**

[14] S. Andriamonje et al., to be published in Nucl.Intr.and Meth.**B.**

[15] A. Doyle and I. Turner, Acta Cristal. **A24** (1968) 390.

[16] J. Lindhard, Mat. Fys. Medd. Dan. Vid. Selsk. **34** n^o 14 (1965).

[17] J.H. Barrett, Phys.Rev.**B3** (1971) 1527.

[18] E. Bonderup, H. Esbensen, J.U. Andersen and H.E. Schiott, Rad.Eff.**12**(1972)261.

[19] H.E. Schiott, E. Bonderup, J.U. Andersen and H. Esbensen, in *Atomic Collisions in Solids vol 2*, edited by S. Datz, B.R. Appleton and C.D. Moak, (Plenum Press, New York, 1975), , p. 843.

[20] C.F. Bunge, J.A. Barrientos and A.V. Bunge, At.Data Nucl.Data Tables **53** (1983) 113.

[21] J.R. Chelikovsky and M.L. Cohen, Phys. Rev. **B14** (1976) 556.

[22] F. Biggs, L.B. Mandelsohn and J.B. Mann, At.Data Nucl.Data Tables**16** (1975) 201.

[23] N. Sakai, N. Shiotani, F. Itoh, O. Mao, M. Ito, H .Kawata, Y. Amemya et M. Ando, J.Phys.Soc.Jpn **58** (1989) 3270.

[24] M. Stobbe, Ann.Physik **7**(1930) 661.

[25] E. Spindler, H.D. Betz and F. Bell, Phys.Rev.Lett. **42** (1979) 832.

[26] K. Bernhardi, E. Haug and K. Wiesemann, At.Data Nucl.Data Tables **28** (1986) 461.

[27] R. Anholt, C. Stoller, J.D. Molitoris, D.W. Spooner, E. Morenzoni, S. Andriamonje, W.E. Meyerhof, H. Bowman, J.S. Xu, Z.Z. Xu, J.O. Rasmussen and D.H.H. Hoffmann, Phys.Rev. **A33** (1986) 2270.

[28] H.W. Koch and J.W. Motz, Rev.Mod.Phys.**31** (1959) 920.

[29] L. Pages, E. Bertel, H. Joffre and L. Sklavenitis, At.Data **4** (1972) 1.

[30] Th. Stöhlker, C. Kozhuharov, P.H. Mokler, A. Warczak, F. Bosch, H. Geissel, R. Moshammer, C. Scheidenberger, J. Eichler, A. Ichihara, T. Shirai, Z. Stachura and P. Rymuza, Phys.Rev. **A51** (1995) 2098.

[31] J.M. Pitarke, R.H. Ritchie and P.M. Echenique, Phys.Rev. **B43** (1991) 62.

FIGURE CAPTIONS

figure 1 : scheme of the experimental setup.

figure 2 : charge state distributions obtained for Kr^{q+} incident ions (q=33, 35, 36) at 60.1 MeV/u on a 37 μm Si crystal for alignment along the <110> direction. The dashed curve corresponds to a calculation for random orientation [13].

figure 3 : single spectra corresponding to all the photons detected at 90° for 60.1 MeV/u Kr^{36+} ions incident on a 37 μm silicon crystal.

figure 4 : photon spectrum recorded at 90° for 60.1 MeV/u Kr^{36+} incident ions in coincidence with well channeled ions which have captured one electron inside the 37 μm silicon crystal aligned along the <110> axis. The corresponding single spectrum is also shown.

figure 5 : simulation of impact parameter distributions $\Phi(b, \psi_0)$ relative to the nearest atomic strings, obtained for different incident angles ψ_0. Dotted curve : $\psi_0 = 0$, no beam angular divergence and no multiple scattering. Dashed curve : random incidence. In the other curves one takes into account a beam angular divergence of 0.1 *mrad* (HWHM) and multiple scattering. Solid line : $\psi_0 = 0$. Dash-dotted curve : $\psi_0 = 0.03°$.

figure 6 : comparison between the K-REC yield $bP_{K-REC}(b)$, from ref. [12] (dashed curve) for the capture of L Si electrons by 25 MeV/u Xe^{53+} ions at given impact parameter b to $b\bar{\rho}_L(b)$ (solid curve). $\bar{\rho}_L(b)$ is the mean L-electron density at b (see eq. (1)).

figure 7 : mean sampled electron density distribution $g(b, \psi_0)$ (solid lines) for 3 different incidence angles ψ_0. Mean electron densities $\bar{\rho}_{st}(b)$ (dotted lines).

figure 8 : map of the mean valence electron density $\bar{\rho}_{val}(\vec{r}_\perp)$ averaged along z. Densities in electron per $Å^3$: 1: 0.032 , 2: 0.08 , 3: 0.15 , 4: 0.225, 5: 0.275, 6: 0.35, 7: 0.45 . The black circles represent the position of the <110> atomic strings.

figure 9 : shape of the momentum distributions $F_{nl}(p_z;\psi_0)$ of $2s$ (a) and $2p$ (b) electrons captured for beams incident at various ψ_0. Solid line : random orientation ; dashed line : $\psi_0 = 0.03°$; dotted line : $\psi_0 = 0$. Multiplying factors were applied to bring the curves together at $p_z = 0$. Electron momenta are converted into REC photon energies.

figure 10 : comparison of Compton profiles $C_{p1}(p_z \mid b)$ (dashed lines) and $C_{p2}(p_z \mid b)$ (solid lines) (see text) at various impact parameters b. Electron momenta are converted into REC photon energies.

figure 11 : comparison of valence momentum distributions $F_{val-random}(p_z)$ uniformly averaged over the transverse space (uniform flux). Dotted line : $F_{val-random}(p_z)$ from ref. [23] ; solid line : $F_{val-random}(p_z)$ from a non uniform Fermi gas description of valence electrons.

figure 12 : decomposition of the single X-ray spectra of fig. 3. The dashed line represents the sum of the various simulated contributions.

figure 13 : channeling dips for K-REC. (a) silicon valence electron contribution ; the curves correspond to simulations for various beam angular divergences ; (b) core electron contribution ; the calculated dips corresponding to various states are represented ; the beam angular divergence is 0.1 *mrad* HWHM. The calculated and experimental dips in (a) and (b) are normalized to the random K-REC calculated yield.

figure 14 : comparison of the K-REC line shape in the coincidence spectrum of fig. 4 (solid line) to : (a) the REC line associated to the valence electron Compton profile measured in ref. [23] (dashed line). (b) The REC line obtained from a Monte-Carlo simulation with a non uniform Fermi gas description of valence electrons (dashed line). The calculated core electron small contribution is also represented.

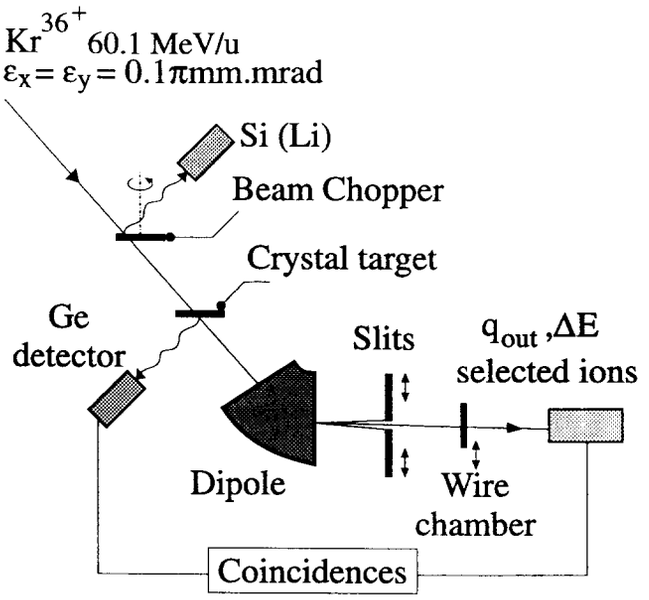

figure 1

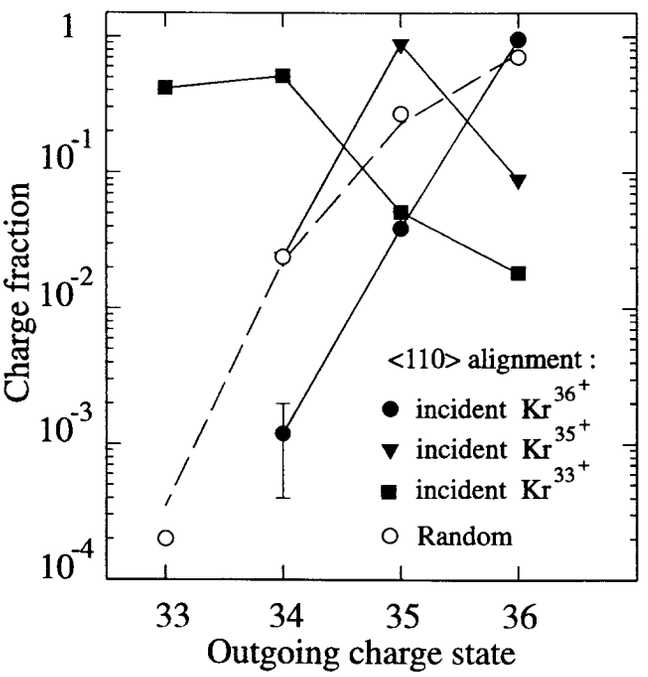

figure 2

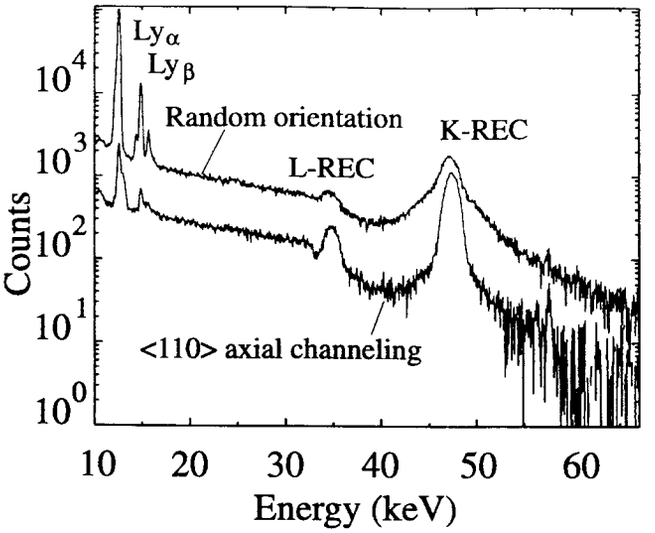

figure 3

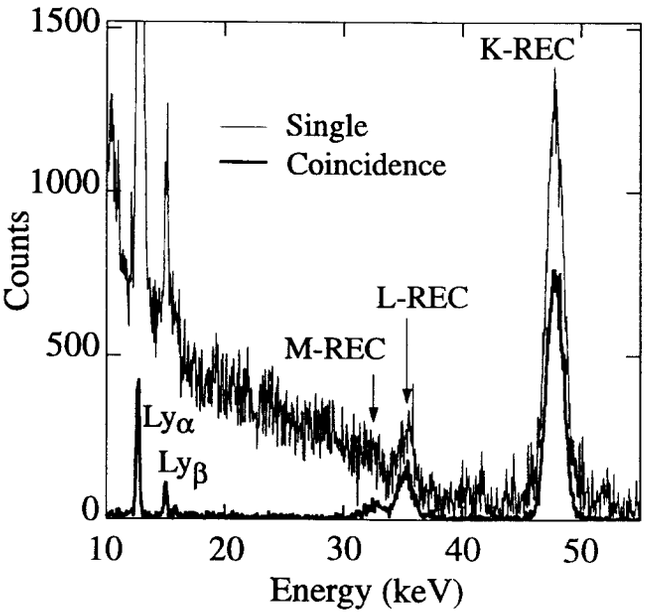

figure 4

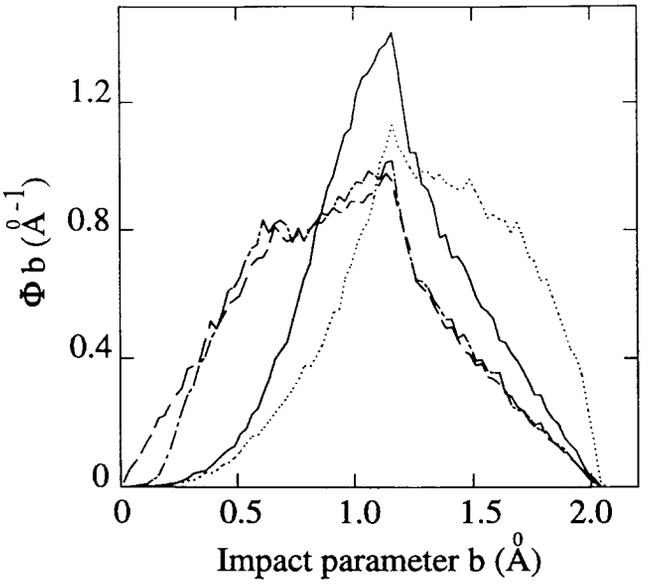

figure 5

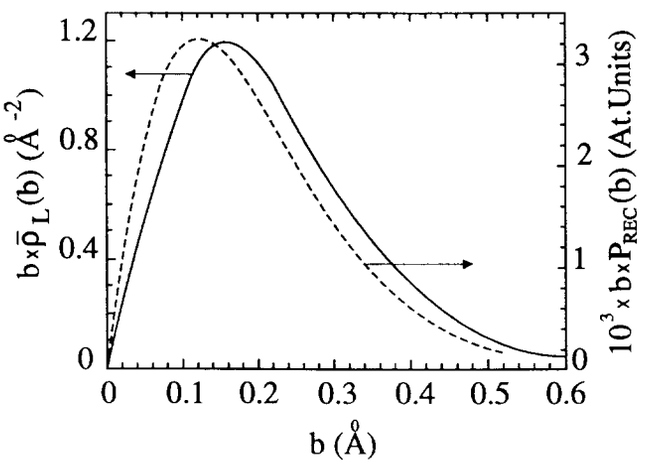

figure 6

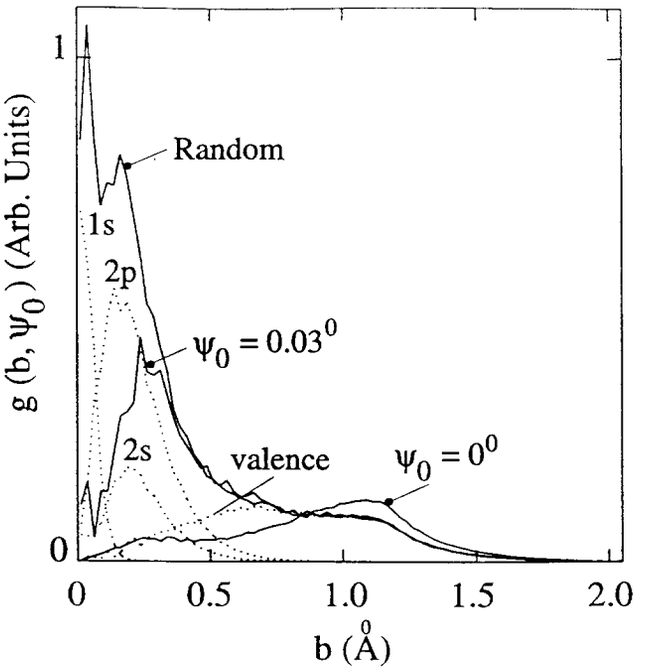

figure 7

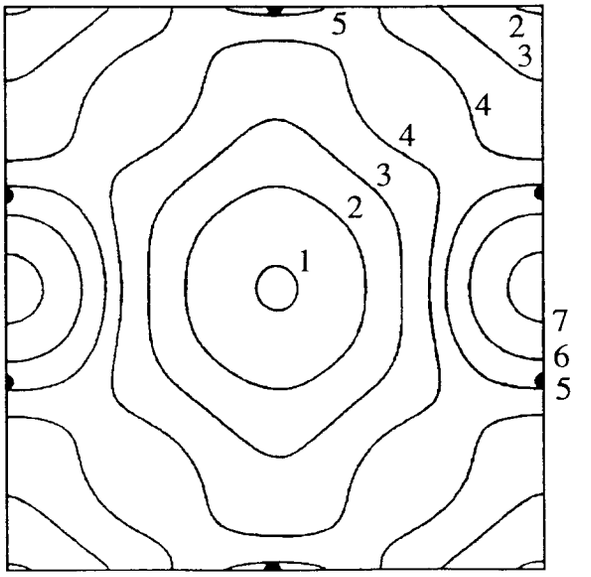

figure 8

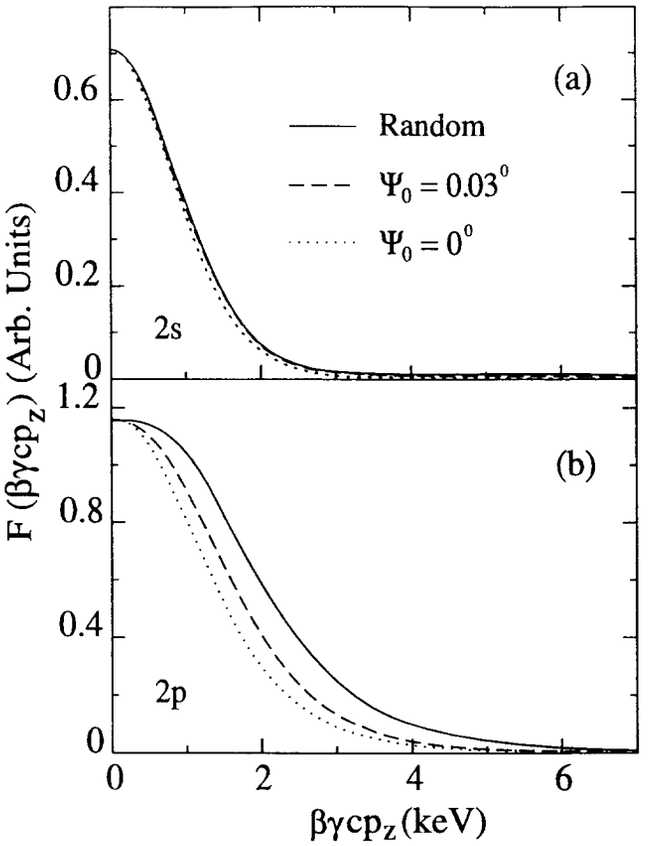
(a)
Random
$\Psi_0 = 0.03^0$
$\Psi_0 = 0^0$
2s
(b)
2p
0.6
0.4
0.2
0
1.2
0.8
0.4
0
0
2
4
6
F ($\beta\gamma cp_z$) (Arb. Units)
$\beta\gamma cp_z$ (keV)

figure 9

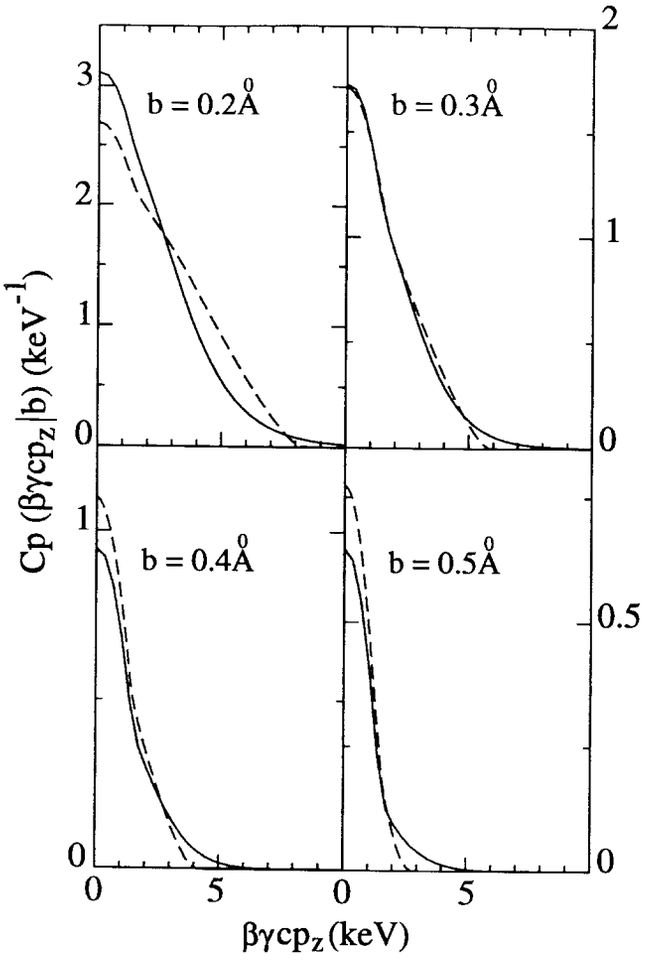

figure 10

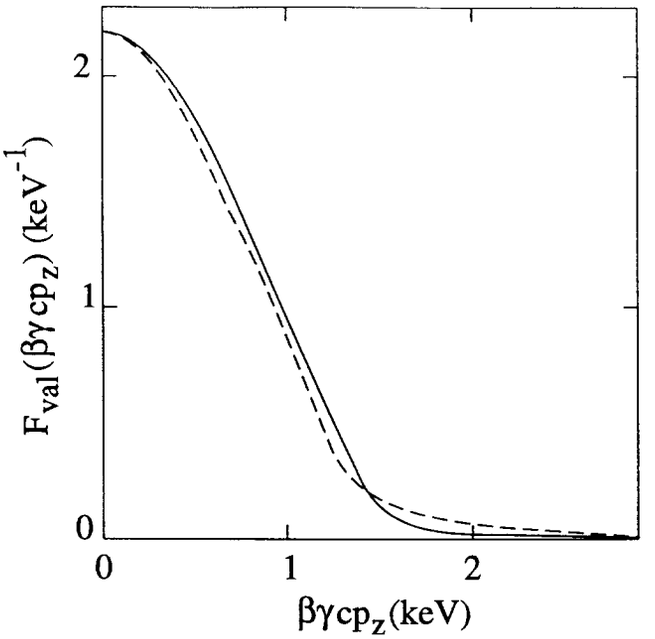

figure 11

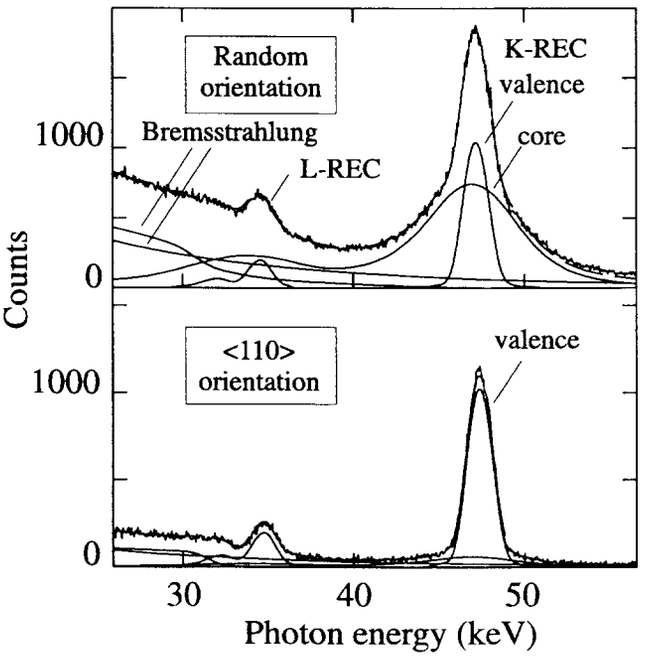

figure 12

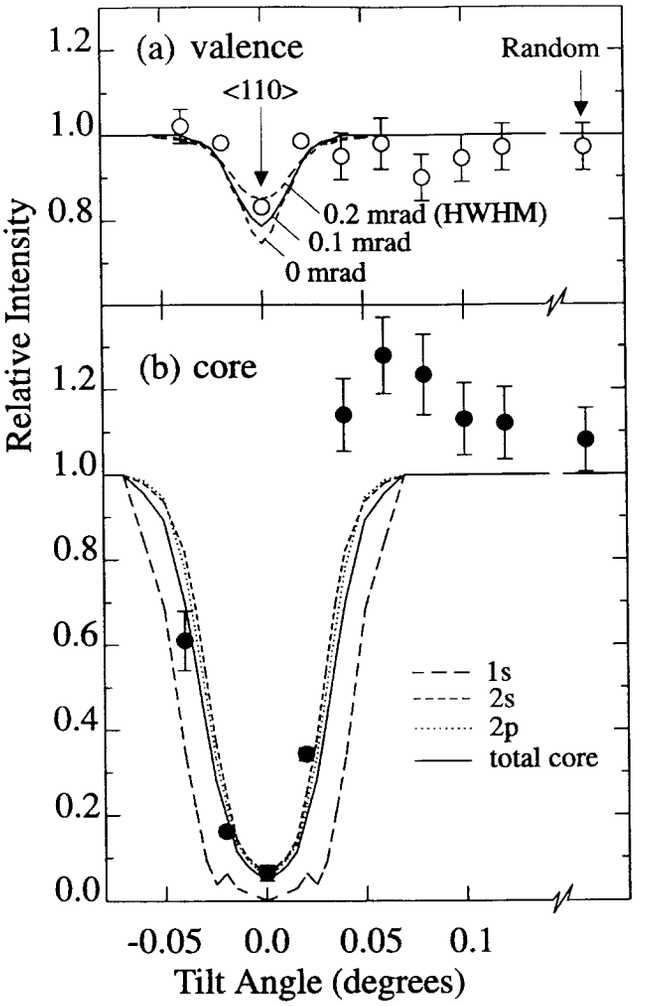
(a) valence
<110>
Random
0.2 mrad (HWHM)
0.1 mrad
0 mrad
(b) core
1s
2s
2p
total core
Relative Intensity
Tilt Angle (degrees)
1.2
1.0
0.8
0.6
0.4
0.2
0.0
-0.05
0.0
0.05
0.1

figure 13

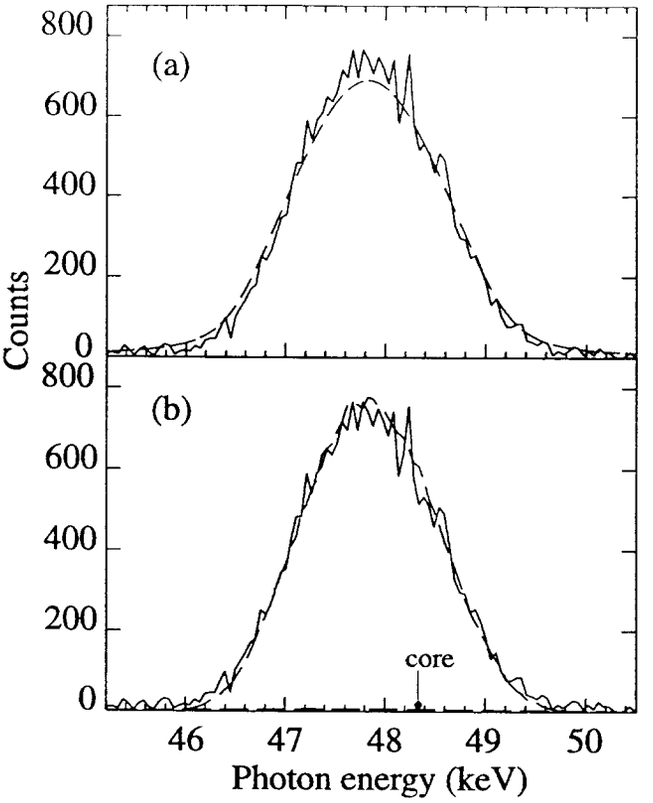
800
600
400
200
0
Counts
(a)
800
600
400
200
0
(b)
core
46
47
48
49
50
Photon energy (keV)

figure 14